Study of a Magnetic Suspended Flywheel Energy Storage System for Pulsed Power

Haoze Wang [a,b], Kun Liu [a]

[a] School of Aeronautics and Astronautics SUN YAT-SEN University, No. 135, Xingang Xi Road, GuangZhou, China, st7715@126.com (specify for at least one author)
[b] Candela (Shenzhen) Technology Innovate Co.Ltd , BingHai Road 3012, Shenzhne, China

***Abstract*—Flywheel Energy Storage Systems (FESS) are found in a variety of applications ranging from grid-connected energy management to uninterruptible power supplies. This article describes the application of FESS in high pulsed power area. The rotor of FESS for puled power is generally supported by the traditional bearings, which are considered as a source of friction during rotation, and require lubrication and high maintenance, and can't be used at high speed ranges. In this paper, a magnetic suspended flywheel energy storage system (MSFESS) is proposed and designed for the pulsed power applications. Topology, principle and discharging model of the MSFESS are introduced and studied. The impacts of the high power pulsed discharge on the magnetic bearing system are analyzed. Scaled prototype of the MSFESS is manufactured and tested.**

I. INTRODUCTION

Flywheel Energy Storage Systems (FESS) are found in a variety of applications ranging from grid-connected energy management to uninterruptible power supplies [1-3] With the progress of technology, there is fast renovation involved in FESS application. Examples include high power weapons, aircraft powertrains and shipboard power systems [4-6], where the system requires a very high-power for a short period in order of a few seconds and even milliseconds.

The develop of pulsed alternators for use as rail gun power supplies in the University of Texas at Austin--Center for Electromechanics has resulted in the evolution of multiple generations of them in the past few decades [7-10]. The strongest machine performs with an output power of 2.5 GW, with the stored insert energy of 40 MJ.

However, FESS for puled power is generally supported by the traditional bearings. Traditional bearings (mechanical bearings) as ball, roller or sleeve bearings are the simplest form of bearings, which are inexpensive and can be easily installed. Nevertheless, they are considered as a source of friction during rotation, and require lubrication and high maintenance. What's more, they should be used at low speed ranges, which limited the energy density of the FESS.

Magnetic bearings utilize magnetic forces to support a rotor. Because of the contactless operating characteristic, they are promising for applications at high speed and in vacuum environments. Moreover, the FESS rotor can be actively controlled by a vibration suppressing algorithm.

In this paper, a magnetic suspended flywheel energy storage system (MSFESS) is proposed and designed for the pulsed power applications. Topology, principle and discharging model of the MSFESS are introduced and studied. The impacts of the high power pulsed discharge on the magnetic bearing system are analyzed. Scaled prototype of the MSFESS is manufactured and tested.

II. STRUCTURE AND PRINCIPLE OF THE MSFESS

The solid assembly model of the MSFESS is shown in Fig. 1. As is shown, the MSFESS is constructed by the vacuum housing, the outer composited flywheel ring, the hybrid magnetic bearing system, the pulsed alternator, the stationary shaft, and the back-up bearings. Energy is stored in the running rotor in the form of rotational inertia and is delivered to an external load in the form of a pulsed current.

An external shell rotor topology is adopted in this system. High-strength carbon fiber/epoxy composite outer band is adopted to restrain the centrifugal radial growth of the rotor throughout the operational rotational speed range. The advantage of this novel topology is not only that it provides the highest energy density of any topology for the highest inertia portion of the alternator is rotating, which makes the system extremely compact, but also that the rotor yoke serves as the structural support for the rotating PMs, which can protect the rotor being damaged by the spin loads of the PMs at very high rotating speed. In addition, the fabrication of the external rotor is very simple, interference fits or structural bandings are not necessary to keep the structure which is accomplished by the centrifugal force instead.

The external rotor topology shown is very efficient in terms of maximizing energy stored per unit weight, but creates challenging bearing requirements. Magnetic bearings appear to be the only type compatible with the requirements for the flywheel storage system. PM bias homopolar magnetic bearings were selected for this FESS, on studies showing increase the rotor speed and lower losses compared to traditional bearings.

The hybrid bearing system configuration chosen consists of two radial MB used on each end of the rotor, which support the rotor in the radial direction actively and in the axial direction passively.

A novel permanent magnet (PM) compensated pulsed alternator is designed for this FESS. The machine is intentionally designed to maximize the output current by minimizing the internal impedance of the armature winding through the action of flux compression.

1. Vacuum Housing
2. Composite Flywheel
3. External Rotor Core
4. Permanent Magnets
5. Compensated Shield
6. Armature Windings
7. Stator Core
8. End Shield
9. Electromagnetic Shield
10. Magnetic Bearing System
11. Back-up Bearing
12. Stationary Axle

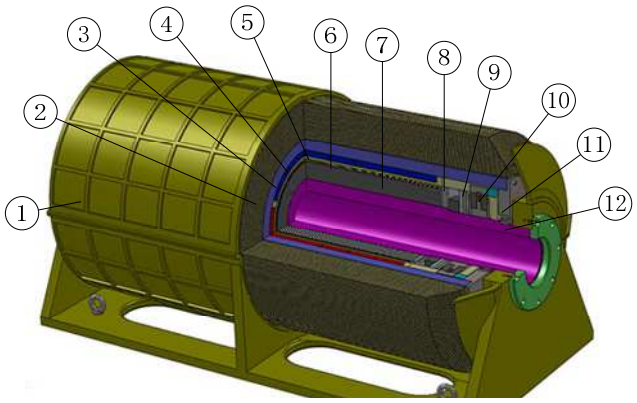

Figure 1. Solid assembly model of the FESS

What is more, the PM pulsed alternator acts not only as a pulsed alternator, which can deliver high pulsed power, but also as a PM BLDC motor, which can be employed to charge the energy storage rotor. Thus, either external driving motor or gearbox is not needed, which makes the system much more compact, lightweight and reliable.

Two backup bearings are configurated for exceed loads, as well as a high efficiency and simple cooling system for vacuum-compatible.

III. MAGNETIC BEARING SYSTEM DESIGN

A. *Magnetic Bearing structure*

In addition to dealing with rotor static and dynamic loads common to all FESS, the bearing system in the FESS for pulsed power must accommodate the shock loads caused by the unbalance magnetic pull and push while discharging.

To reduce the idle losses and enable the flywheel to meet the long lift requirement, the flywheel rotor must operate in a vacuum, and the friction of the bearing must be minimized.

A novel external rotor PM bias homopolar magnetic bearings were selected for this FESS to reduce power losses and enlarge the load capacity. The schematic of this kind of hybrid magnetic bearing is shown in Fig. 2. The stator consists of a PM ring sandwiched between two magnetic flux plates. Each magnetic flux plate contains four poles, 8 electromagnetic coils are symmetrically wounded on this poles. The conducts of the coils are filled in the slots of the flux plates. The rotor is concentric with the stator and is separated from it by two small air gap.

PM is used to provide bias flux (see Fig.2). Position transducers located at the periphery of the stator get the eccentricity of the rotor; the bias flux in the suspension air gap of the bearing is modulated by control flux produced by the electromagnetic coils. This composite flux develops restore force, stabilizes the rotor in the radial direction and maintains a uniform air gap.

B. *Analytic Model of the Magnetic Bearing*

Based on the structure of Fig.2, the equivalent magnetic circuit of the bias flux and the control flux of the y-axis of the HMB is shown in Fig. 3, which is similar in x-axis. It is easy to assume that the control current in x direction coils is i_x and the control current in y direction coils is i_y .

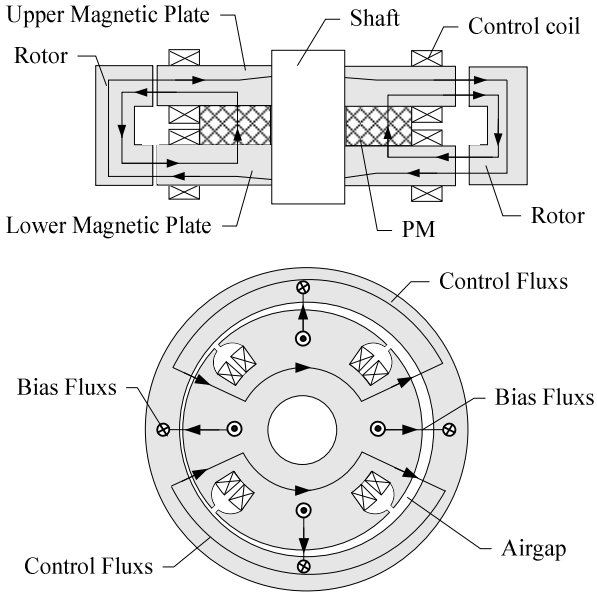

Figure 2. The schematic of the HMB include the flux path. The cross-section view (upper), the top view (lower)

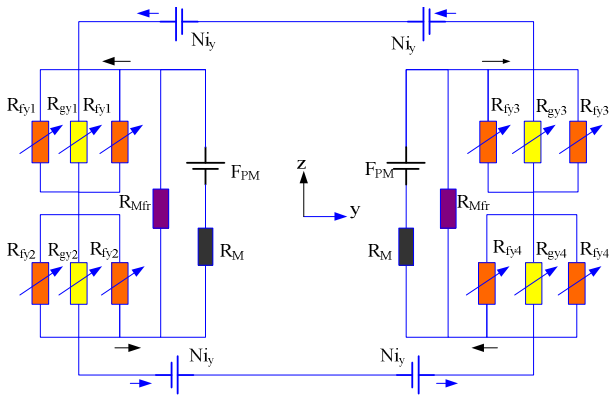

Figure 3. The equivalent magnetic circuit of the HMB

Hence, the following equations of the whole HMB can be

achieved:

$$\begin{cases} F_{cx} = 4Ni_x = \Phi_{gex1}R_{gx1} + \Phi_{gex2}R_{gx2} + \Phi_{gex3}R_{gx3} + \Phi_{gex4}R_{gx4} \\ F_{cy} = 4Ni_y = \Phi_{gey1}R_{gy1} + \Phi_{gey2}R_{gy2} + \Phi_{gey3}R_{gy3} + \Phi_{gey4}R_{gy4} \\ F_{PMx} = H_c h_{Mx} = \Phi_{Mx}R_{Mx} + \Phi_{gMx1}R_{gx1} + \Phi_{gMx2}R_{gx2} \\ F_{PMy} = H_c h_{My} = \Phi_{My}R_{My} + \Phi_{gMy1}R_{gy1} + \Phi_{gMy2}R_{gy2} \\ \Phi_{Mx} = \Phi_{Mfx} + \Phi_{gMx1} + 2\Phi_{gMfx1} \\ \Phi_{My} = \Phi_{Mfy} + \Phi_{gMy1} + 2\Phi_{gMfy1} \end{cases} \quad (1)$$

F_{cx}, F_{cy} are MMFs of the control current in x, y axis, F_{PMx}, F_{PMy} are MMFs of the PM, N is the turns of each coil, and as shown in Fig. 2, there is 4 coils in each direction. $\Phi_{gex1}, \Phi_{gey1} \cdots\cdots \Phi_{gex4}, \Phi_{gey4}$ are control flux in each air gap, Φ_{Mx}, Φ_{My} are total flux stream through the PM, $\Phi_{gMx1}, \Phi_{gMx2}, \Phi_{gMy1}, \Phi_{gMy2}$ are bias flux in each air gap, $\Phi_{gMfx1}, \Phi_{gMfy1}$ are fringing flux in the air gap, Φ_{Mfx}, Φ_{Mfy} are leak flux of the magnetic circuit except in the air gap, $R_{gx1}, R_{gy1} \cdots$ are reluctances in each air gap, R_{Mx}, R_{My} are reluctance of the PM, H_c is the coercive force of the PM, h_{Mx}, h_{My} are lengths of the PM. Φ_{Mfx}, Φ_{Mfy} are fringing flux of the magnetic circuit except $\Phi_{gMfx1}, \Phi_{gMfy1}$, and the coefficient of flux leakage is σ_M, which is assumed to be constant actually. For the symmetry of the structure of the hybrid MB, $\Phi_{gex1} = \Phi_{gex2} = \Phi_{gex3} = \Phi_{gex4}$, $R_{gx1} = R_{gx2} = R_{gx3} = R_{gx4}$, $\Phi_{gey1} = \Phi_{gey2} = \Phi_{gey3} = \Phi_{gey4}$, $R_{gy1} = R_{gy2} = R_{gy3} = R_{gy4}$.

So:

$$\begin{cases} \Omega_{x1} = \Omega_{x2} = Ni_x + \dfrac{H_c h_M}{\dfrac{\sigma_M}{K_g(\sigma_M - 1)}\dfrac{2\mu_0\theta R h_M h}{\mu_M A_M \delta} + 2} \\ \Omega_{x3} = \Omega_{x4} = -Ni_x + \dfrac{H_c h_M}{\dfrac{\sigma_M}{K_g(\sigma_M - 1)}\dfrac{2\mu_0\theta R h_M h}{\mu_M A_M \delta} + 2} \\ \Omega_{y1} = \Omega_{y2} = Ni_y + \dfrac{H_c h_M}{\dfrac{\sigma_M}{K_g(\sigma_M - 1)}\dfrac{2\mu_0\theta R h_M h}{\mu_M A_M \delta} + 2} \\ \Omega_{y3} = \Omega_{y4} = -Ni_y + \dfrac{H_c h_M}{\dfrac{\sigma_M}{K_g(\sigma_M - 1)}\dfrac{2\mu_0\theta R h_M h}{\mu_M A_M \delta} + 2} \end{cases} \quad (2)$$

$\Omega_{x1}\Omega_{y1}, \cdots \Omega_{x4}, \Omega_{y4}$ are MMFs drop in each air gap, μ_M is the permeability of the PM, μ_0 is the permeability of free space, A_M is the air of each PM, A_g is the pole air, R is the outer radius of the magnetic poles, θ is the pole angle, h is the height of the flux plate, K_g is the coefficient of the air gap($\sigma = 1/K_g$ is the coefficient of air gap flux leak), which is expresses in literature [11], as

$$K_g = 1 - \frac{\delta}{\pi h}\left|(\frac{(d-1)}{4\sqrt{d}} - \frac{1}{2})\pi j - \ln d - \frac{\pi}{2}\right| \quad (3)$$

where δ is the length of the air gap, $\sqrt{d}$ is the structure coefficient of the MB, $\sqrt{d} = \sqrt{1+(\Delta/\delta)^2} - \Delta/\delta$, Δ is the axial misaligned between the stator and the rotor.

Because of the iron boundary of infinite permeability, the field strength in it is zero and all the energy is stored in the air space. And the magnetic force is the rate of change of the stored energy in the air gap. So, The radial restore magnetic force in radial directions of x, y axis can be integrated along the bearing circumference, described as follow:

$$\begin{aligned} F_x = & 2\int_{-\frac{\beta}{2}}^{\frac{\beta}{2}} \frac{\mu_0 R\Omega_{x1}^2}{\pi\delta}[\frac{\pi h}{\delta} - 1]\cos\theta d\theta \\ & + 2\int_{\pi-\frac{\beta}{2}}^{\pi+\frac{\beta}{2}} \frac{\mu_0 R\Omega_{x3}^2}{\delta\pi}[\frac{\pi h}{\delta} - 1]\cos\theta d\theta \\ & + 2\int_{\frac{\pi}{2}-\frac{\beta}{2}}^{\frac{\pi}{2}+\frac{\beta}{2}} \frac{\mu_0 R\Omega_{y1}^2}{\pi\delta}[\frac{\pi h}{\delta} - 1]\cos\theta d\theta \\ & + 2\int_{\frac{3\pi}{2}-\frac{\beta}{2}}^{\frac{3\pi}{2}+\frac{\beta}{2}} \frac{\mu_0 R\Omega_{y3}^2}{\pi\delta}[\frac{\pi h}{\delta} - 1]\cos\theta d\theta \end{aligned} \quad (4)$$

$$\begin{aligned} F_y = & 2\int_{-\frac{\beta}{2}}^{\frac{\beta}{2}} \frac{\mu_0 R\Omega_{x1}^2}{\pi\delta}[\frac{\pi h}{\delta} - 1]\sin\theta d\theta \\ & + 2\int_{\pi-\frac{\beta}{2}}^{\pi+\frac{\beta}{2}} \frac{\mu_0 R\Omega_{x3}^2}{\delta\pi}[1 - \frac{\pi h}{\delta}]\sin\theta d\theta \\ & + 2\int_{\frac{\pi}{2}-\frac{\beta}{2}}^{\frac{\pi}{2}+\frac{\beta}{2}} \frac{\mu_0 R\Omega_{y1}^2}{\pi\delta}[\frac{\pi h}{\delta} - 1]\sin\theta d\theta \\ & + 2\int_{\frac{3\pi}{2}-\frac{\beta}{2}}^{\frac{3\pi}{2}+\frac{\beta}{2}} \frac{\mu_0 R\Omega_{y3}^2}{\pi\delta}[\frac{\pi h}{\delta} - 1]\sin\theta d\theta \end{aligned} \quad (5)$$

β is the pole angle.

IV. PULSED ALTERNATOR AND PULSE CUTTENT SWITCH

A. Novel PM Pulsed Alternator

Briefly, the novel PM pulsed alternator is typically a special external rotor brushless DC motor/alternator with a shield Component. The shield shell is intentionally designed to maximize the current output by minimizing the internal inductance of the armature through the action of passive flux compression.

As shown in Fig. 4, the alternator is constructed by the internal stator and the external rotor. The internal stator is consisted of the slotless stator core and the armature windings. There are 4 surface-mounted one-layer armature windings arranged on the outer surface of the core which constitute the 4 pole 2 phase windings. Surface mounted permanent magnets are chosen to reduce the manufacturing cost, which are adhered on the inner surface of the rotor yoke. Conductive

shield is located on the inner surface of the PMs, which compress the armature reacted flux to minimize the inductance of the armature as well as to protect the PMs from being demagnetized.

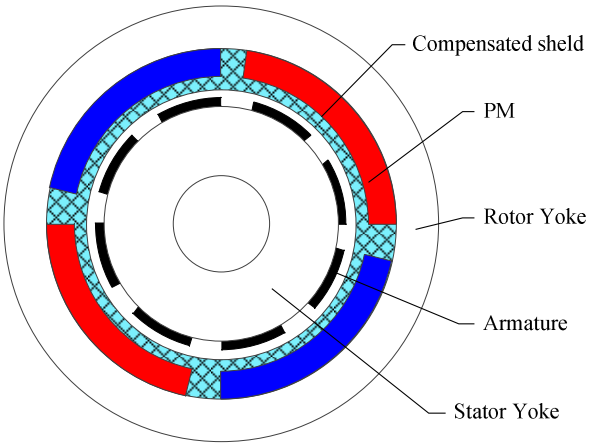

Figure 4. radial cross-sectional view of the novel PMPA

Similar to the traditional alternator, PMs are employed to provide the exciting flux. Cyclic voltage is induced through the relative motion between the armature and the exciting magnetic field. Energy is delivered to an external load as the form of current. The armature reactive fluxes produced by the load current are compressed in the air gap between the stator and the shield shell. Reluctance of the flux circuit is increased dramatically, and the inductance of the armature is minimized greatly which makes the output current grow rapidly.

B. Model of the PM Pulsed Alternator

The open-circuit phase voltage induced in the stator armatures by varying the magnetic field in the air gap is known as the EMF. The output voltage of the two phases of the machine at any given moment in time can be analytically found by using Farady's law, which is expressed as

$$\begin{cases} E_A(t) = 2pR_w l_e \omega \sum_{n=1,2,3\cdots}^{N_A} \sum_{\nu=1,3,5\cdots}^{\infty} \left[K_m^{(\nu)} \cdot A^{(\nu)} \cdot B_r^{(\nu)}(R_w) \right. \\ \qquad \left. \cdot \sin \nu p\theta_{nA} \cdot \sin \nu p(\omega t + \gamma_0) \right] \\ E_B(t) = 2pR_w l_e \omega \sum_{n=1,2,3\cdots}^{N_A} \sum_{\nu=1,3,5\cdots}^{\infty} \left[K_m^{(\nu)} \cdot A^{(\nu)} \cdot B_r^{(\nu)}(R_w) \right. \\ \qquad \left. \cdot \sin \nu p\theta_{nA} \cdot \sin \nu p(\omega t + \gamma_0 - \frac{\pi}{2p}) \right] \end{cases}$$

Where

$$K_m^{(\nu)} = \frac{4pB_r}{\pi[(\nu p)^2 - 1]} \sin \frac{\nu \pi \alpha_p}{2}$$

$$A^{(\nu)} = \frac{(\nu p - 1)(\frac{R_m}{R_r})^{2\nu p} + 2(\frac{R_m}{R_r})^{\nu p - 1} - \nu p - 1}{(\mu_M + 1)\left[1 - (\frac{R_s}{R_r})^{2\nu p}\right] - (\mu_M - 1)\left[(\frac{R_s}{R_m})^{2\nu p} - (\frac{R_m}{R_r})^{2\nu p}\right]}$$

$$B_r^{(\nu)}(r) = (\frac{r}{R_m})^{\nu p - 1} + (\frac{R_s}{R_m})^{\nu p - 1}(\frac{R_s}{r})^{\nu p + 1}$$

$$B_t^{(\nu)}(r) = (\frac{r}{R_m})^{\nu p - 1} - (\frac{R_s}{R_m})^{\nu p - 1}(\frac{R_s}{r})^{\nu p + 1}$$

ν is the harmonic number which can be written as $\nu = 2n-1$, $n \in Z$, a_p is the magnet pole-arc to pole-pitch ratio, p is the number of pole-pairs, Rs, Rm, Rr are the radii of the stator, magnets and the inner surface of rotor, respectively. Rw is the average radius of the armature winding, $Rw = (Rs + Ra)/2$, le is the effective axial length of the stator, γ is the rotor positional angle with respect to the stator fixed reference axis, $\gamma = \omega t + \gamma 0$, ω is the rotor angular velocity, $\gamma 0$ is the initial rotor positional angle. N_A the number of turns in each coil, $2\theta_{nA}$ is the span angle of any winding turn in one coil, μ_M is the relative recoil permeability of the PMs.

Substitute the initial current of i (0+) = i(0-) = 0, the short-circuited discharge current of any phase can be deduced as

$$i(t) = 2pR_w l_e \omega \sum_{\nu=1,3,5\cdots}^{\infty} \sum_{n=1,2,3\cdots}^{N_A} \frac{K_m^{(\nu)} \cdot A^{(\nu)} \cdot B_r^{(\nu)}(R_w)}{|Z|} \cdot \sin \nu p\theta_{nA}$$
$$\cdot \left[\sin(\nu p\omega t + \nu p\gamma_0 - \varphi^{(\nu)}) - \sin(\nu p\gamma_0 - \varphi^{(\nu)}) \cdot e^{-\frac{t}{\tau}} \right]$$

Where $\tau = L/R$, $\varphi^{(\nu)} = \arctan(\nu p\omega L/R)$, $|Z^{(\nu)}| = \sqrt{R^2 + \nu^2 p^2 \omega^2 L^2}$, τ is the time constant of the circuit, φ *is* the phase delay of the discharge circuit and, , $|Z^{(\nu)}|$ is the module of the internal impedance of the machine in any frequency.

V. THE IMPACTS OF THE PULSE DISCHARGE ON THE MAGNETIC LEVITATED SYSTEM

Since the invention, the purpose of the flywheel is to damp out changes in speed due to a pulsed motive source or a pulsed load. However, in FESS for puled power system, when a machine is built into an apparatus, the rotor eccentricity is occurred, due to the flux compression, any eccentricity of the rotor or the asymmetry of the armature wingding will induce large unbalance magnetic force, which will bring on electromagnetic shock and great rotor vibration that are not produced in convention flywheel.

The magnitude of these unbalanced electromagnetic forces becomes a driving design consideration for these machines as GW power levels are contemplated.

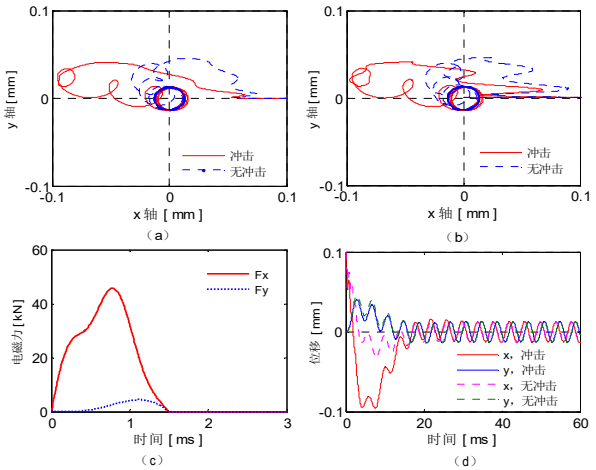

Figure 5. The rotor dynamic response while discharging. (a) (b) the orbit of shaft center; (c) unbalanced magnetic force; (d) rotor radial

In this paper the model of the unbalanced electromagnetic force is induced, shock response of the rotor system is analyzed. When the initial rotor eccentricity is 0.1 mm, the peak of the pulse current is 50 kA, the rotor dynamic response while discharging is shown in Fig. 5.

As is shown, rotor eccentricity will cause huge unbalanced magnet pull or push while discharging which make the rotor acceleration. Due to the shock isolate of the magnetic bearing , the transmitted rotor shock is eliminated, and the rotor displacement is below the backup bearing clearance of 0.2 mm. The rotor is safe.

The analytical model of the unbalance magnetic shock and it derivation process has not been presented in this paper for saving space. It will be discussed in another article.

VI. PROTOTYPE TEST OF THE MSFESS

A. Prototype of the FESS

A prototype has constructed with the aim of addressing the critical technical challenges of the MSFESS for puled power. The photograph of the scaled prototype is shown in Fig. 6. As may be apparent, the carbon fiber/epoxy composite outer band was not adopted, in order to reduce the budget. The basic design parameters of the scaled prototype are shown in Tables I. The overall dimensions of the rotor whose mass is 125 kg, the deliverable rotational inertial energy of the outer rotor over 2 MJ at a rotor speed of 12 000 r/min. The peak power output is 9.5MVA with a phase voltage of 380V.

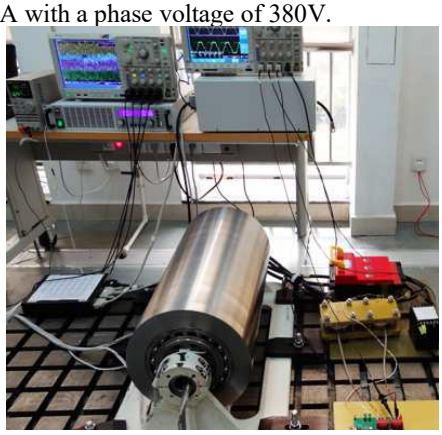

Figure 6. Photo of the prototype of the FESS

TABLE I. PARAMETERS OF THE SCALE-MODEL PROTOTYPE

Parameters	Value	Unit
Rated rotor speed	12000	rpm
Energy storage	2.05	MJ
Peak phase voltage	380	V
Peak current	18.5	KA
Phase number	2	
Electrical frequency	400	Hz
Outer diameter of the stator	0.2	m
Outer diameter of the rotor	0.3	m
Length of the rotor	0.64	m

B. Magnetic Bearing fabrication

In order to induce the loss of eddy current, the HMB is designed in special construct, the lips of slots in this HMB are connected together, that means the pole angle β is 90º. See Fig. 7, which are parts of the HMB under assembling.

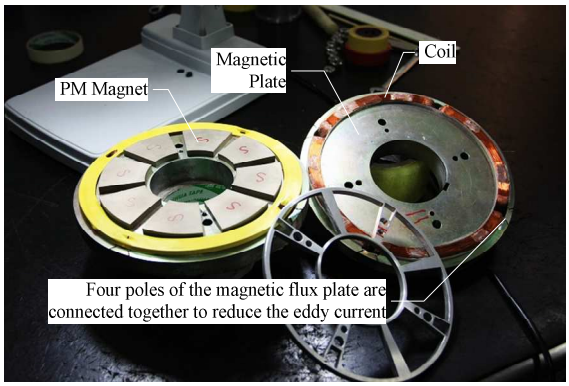

Figure 7. The parts of the HMB

The PM Ring is separated to 8 pieces, the stator magnetic plates is made of pure iron, and the rotor is made of stacked-steel sheet. The design parameter: R=100 mm is the radius of the air gap, δ_0=0.5 mm is the width of the air gap, $2h = 16mm$ is the thickness of the magnetic plates, $B_m = 0.75\,\mathrm{T}$ is the effective bias flux density in the air gap. The output load capacity for one bearing is 4500N, which is 6× g of the rotor.

C. Controller and Solid-State Switch for Pulsed Power

A cautious test plan was designed to analyze the machine's performance and validate the reliability of the system incrementally.

The controller design is centered about the management of the rotor charging and discharging. The process of the rotor charging and discharging is a series of states which is controlled by the micro-control unit (MCU). First, the controller outputs the charging signal to the BLCD driver, the driver drives the motor and accelerates the rotor.

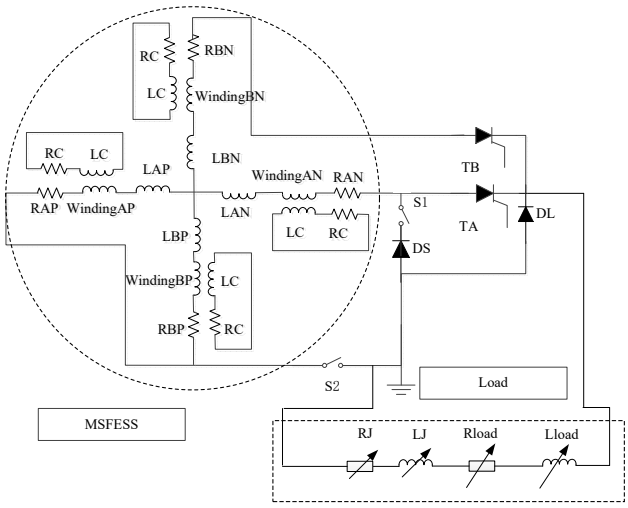

Figure 8. Pulsed Power discharge controller and switches

The controller detects the cross-zero signal of the inducted

phase voltages, calculates the rotor rotating speed and the relative poles position. If the rotor speed achieve the rated speed, the MCU sets the interrupt to the driver, the acceleration process is finished, and the rotor speed is kept constant. The MCU enables the input from the fire switch. After input the discharging signal and the triggering angle, the controller will calculate the discharging time and output triggering pulse to the thyristors. If the firing process has just completed, the MCU sets a driving signal to the BLSM driver, the rotor will accelerated to the rated speed for the next fire.

The pulsed power discharge controller and the solid-state pulsed current switches system is shown in Fig. 8. Large-diameter fast turn-off thyristors are chosen to the discharge circuit, which is controlled by a micro-control unit.

D. Discharge Test

The single phase performance of the scale-model prototype is shown in Fig. 9, which is sampled by a Tek® high speed wide-band-digital oscilloscope. The blue line is the phase voltage wave, the red line is the pulsed current, and the skyblue dashed line is the pulsed current obtained by the analytic method. The sensitivity of the current sensor is 2A/mV.

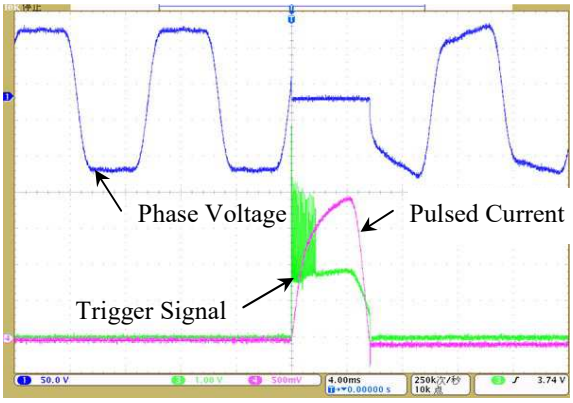

Figure 9. Photo of the prototype of the FESS

As can be seen, the open-circuit phase voltage waveform approximates a trapezoidal wave as prospected by the analytical method. The peak voltage, U = 99 V, was measured at a rotational speed of about 3,000 rpm. The peak value of the pulsed current at short-circuit discharge is about 4.04 kA. The pulse width is about 5.72 ms, which is more than half of the voltage cycle (5 ms).

E. Shock Response of the magnetic suspended rotor

During the system high power discharge, electromagnetic forces produced by rotor eccentricity rapidly shock the rotor and impart a corresponding rotor movement. In a multi-discharge process, the pulsed current is about 6.25 kA, and the pulse width is about 8.84 ms, while the shock response of the magnetic suspended rotor in the prototype is shown in Fig. 10.

As is shown, the maximum radial displacement is 91 um (The sensitivity of the displacement sensor is 8V/mm), while the peak discharging power is 625 kW. The rotor induced a huge unbalanced magnetic force, it accelerated the rotor, and the rotor displacement has finally been eliminated by the magnetic bearing, and the rotor displacement is far below the backup bearing clearance.

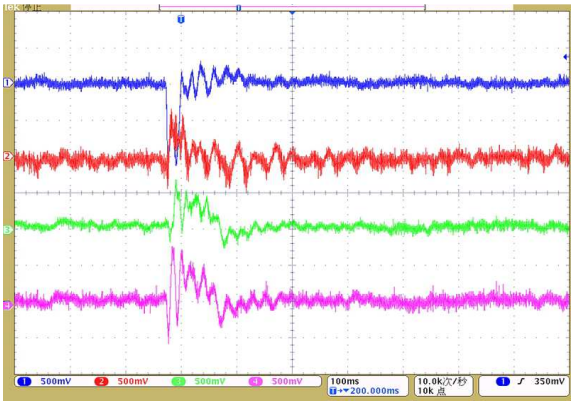

Figure 10. Shok Response of the magnetic suspended rotor

REFERENCES

[1] SEBASTIAN R, PENA-ALZOLA R. Control and simulation of a flywheel energy storage for a wind diesel power system [J]. International Journal of Electrical Power & Energy Systems, 2015, 64(1049-56.

[2] PAN I, DAS S. Kriging Based Surrogate Modeling for Fractional Order Control of Microgrids [J]. IEEE Transactions on Smart Grid, 2015, 6(1): 36-44.

[3] ABRAHAMSSON J, HEDLUND M, KAMF T, et al. High-Speed Kinetic Energy Buffer: Optimization of Composite Shell and Magnetic Bearings [J]. IEEE Transactions on Industrial Electronics, 2014, 61(6): 3012-21.

[4] SWETT D W, BLANCHE J G I. Flywheel charging module for energy storage used in electromagnetic aircraft launch system [J]. IEEE Transactions on Magnetics, 2005, 41(1): 525-8.

[5] MCNAB I R. Large-Scale Pulsed Power Opportunities and Challenges [J]. Ieee T Plasma Sci, 2014, 42(5): 1118-27.

[6] SCUILLER F. Simulation of an energy storage system to compensate pulsed loads on shipboard electric power system; proceedings of the Electric Ship Technologies Symposium (ESTS), 2011 IEEE, F 10-13 April 2011, 2011 [C].

[7] PRATAP S, ZOWARKA R, HOTZ, et al. Synchronization of multiple pulsed alternators discharging into an EM launcher; proceedings of the Electromagnetic Launch Technology (EML), 2014 17th International Symposium on, F 7-11 July 2014, 2014 [C].

[8] BEACH F C, MCNAB I R. Present and Future Naval Applications for Pulsed Power [M]. 18th IEEE InternationalPulsed Power Conference. 2011: 1-7.

[9] CHEN Y Y, SHEPARD N, MALLICK J. Experimental Results from a Physical Scale Model Alternator Pair as a Pulsed Power [J]. IEEE Transactions on Magnetics, 2007, 43(1): 265-9.

[10] KITZMILLER J R, PRATAP S B, DRIGA M D. An application guide for compulsators [J]. IEEE Transactions on Magnetics, 2003, 39(1): 285-8.

[11] Haoze Wang, Kun Liu, Peng Ao. Magnetic Field and Specific Axial Load Capacity of Hybrid Magnetic Bearing [J]. IEEE Transactions on Magnetics, 2013, 49(8):4911-4916.